An Islanding Detection and Control Strategy to Realize the Stable and Autonomous Operation of Microgrids Using the Virtual Synchronous Generator

Illuru Sree Lakshmi[1], Y. Manasa[2]
[1, 2]JNTUA, India

Abstract: An islanding detection and based control strategy is created in this exploration to accomplish the steady and independent activity of microgrids using the neural network based Virtual Synchronous Generator (VSG) idea during unplanned grid reconfigurations . Maybe of utilizing a design-orientedmethodology, this paper gives a rigorous and extensive hypothetical investigation and reaches a concise conclusion that is easy to execute and successful even in complex situations. Based on the results of the mutation sequence and voltage wavering, a neural network based islanding identification calculation is proposed, which requires less constraint strategy. The proposed neural network approach outperforms the thefrequency measured passive detection method in terms of detection speed and reliability. Broad recreations affirm the reasonableness of the proposed islanding location and control methodology. Additionally, think about the results of the reproductions for the PI regulator, fluffy organizations, and neural organizations.
Keywords: Virtual Synchronous Generator, Islanding detection, Islanding operation, Droop control, Stability, Microgrids.

I. INTRODUCTION

Many microgrids have been built with access to distribution networks, where the power flow has been dramatically changed, as a result of the widespread use of renewable energy in daily life. Microgrids, unlike Synchronous Generators (SG) with high overloading-handling capacity, have a hard time dealing with large-scale power imbalances (for example, in islanding operations), which compel the system to shut down owing to protection triggering, resulting in wide-area power outages. As a result, it is critical to detect isolated islands early and take effective actions to ensure the safe and stable operation of microgrids. Due to the difference in generating scale and connectivity degree, when the power grid fails to supply electricity to the distribution lines due to faulty or planned repair, diverse distributed generation units and local loads would generate many unknown islands [1]. This disrupts the planned power balance, posing a significant barrier to the functioning of microgrids connected to distribution systems. As a result, the microgrid system must be able to detect unintended islanding in a reliable and accurate manner. To easily progress to an isolated framework, the framework ought to be turned off from the Point of Common Coupling (PCC) once islanding has been affirmed (e.g., stable activity of the microgrids). The broadly utilized voltage-controlled inverters at the PCC ought to be appropriately changed in this example.

Many Islanding Detection Methods (IDMs) for conventional VSCs have been proposed in the literature, which can be divided into active and passive methods. Active IDMs should actively inject small harmonics to the PCC by monitoring the voltage harmonic change rate [2], average absolute frequency deviation [3], high-frequency transient injection [4], harmonic current disturbance [5,6], and negative sequence power injection [7]. The active IDM can determine if the system is entering the islanding operation when a voltage disturbance is detected at the PCC.

The active IDM, on the other hand, would invariably have an impact on the output power quality as well as the coordination and interaction with other parallel inverters connected to the PCC. To overcome this, in [8,9], the negative sequence component of the voltage signal was utilized to recognize *islanding*, showing that the s-transform has stronger anti-noise abilities than the wavelet change under factor network impedance and PQ unsettling influences. Notwithstanding, during fault ride-through activity, the negative sequence component of the grid voltage vacillates significantly, which could prompt a confusion of the current activity condition. Passive IDMs, then again, are free of *current* working calculations and easy to carry out in equal inverters. The parameter selection for *passive IDMs*, on the other hand, is more difficult [10], and the Non-Detection Zone (NDZ) is typically significantly greater than for active IDMs. Aside from those disadvantages, passive approaches require a longer detection time before the selected electrical characteristics surpass the thresholds in practice.

In light of the foregoing, it may be more practical in some circumstances to mix passive and active IDMs for improved performance. Nonetheless, prior-art approaches for Voltage Source Converters (VSC), which are inertia-free devices, are being developed. The Virtual Synchronous Generator (VSG) concept was established to assure grid stability by making VSCs mirror the behavior of traditional SGs. An IDM index was derived from a frequency deviation in the synchronization process, which indicates sluggish detection speed and reliability, especially under difficult conditions such as low voltage ride-through and minor frequency aberrations (i.e., the required power equals to the rated). In addition, the discrete wavelet transform was used, although it required eight filters and did not include the parameter design. With the aforementioned concerns in mind, this work presents a VSG-based islanding detection and control technique. The weak coupling between the active power-frequency ($P - f$) and the reactive power-voltage amplitude (Q-V) droop characteristics in VSG power loopsshould but cannot be completely cancelled in the VSG parameter designing process, it is revealed that the issues cannot be completely addressed in the VSG design phase.

Furthermore, the order of parameter mutation is highly useful in identifying island phenomena, in contrast to state-of-the-*art passive IDMs* that wait for selected parameters to hit thresholds [7]. To put it another way, the proposed strategy improves dynamics. Only simple reversing logic operations are required for implementation, which is universal and convenient in comparison to sophisticated parameter design and digital operations. Furthermore, two branches are created for each other, one for speedy diagnosis and the other for backup operation, ensuring the detection's reliability.

The following is a list of the paper's main contributions. (1) Rather of using a design-oriented approach, this work presents a rigorous and thorough theoretical study and draws a concise conclusion that is simple to execute and nevertheless useful in complex situations. (2) An *islanding detection* approach that is faster and more reliable is proposed, with no requirement for parameter design. (3) Because the suggested method is based solely on droop characteristics, it may be used to droop-controlled inverters or generators without requiring any new expertise.The innovative control method, in contrast to the well-known Proportional-Integral (PI), deadbeat, and repeating control schemes,does not require reference-frame transformations or PI tuning while maintaining relatively acceptable accuracy. The remainder of this work is arranged in the following manner.

II. BASIC PRINCIPLES OF VSG ALGORITHM

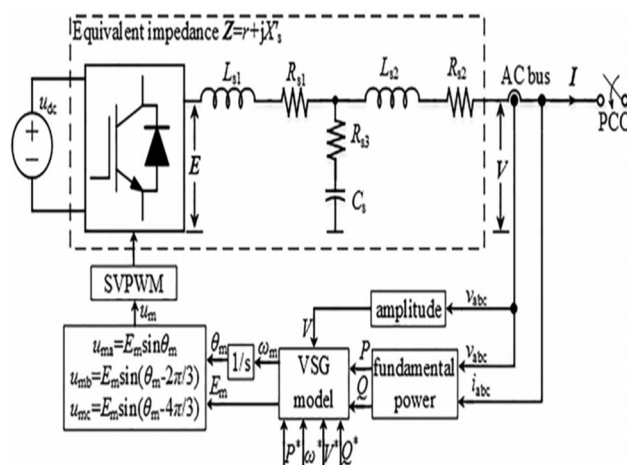Fig.1shows a three-phase inverter with the VSG control.

Fig. 1. A three-phase voltage-source converter with the VSG control,

Where $u_{ma}, u_{mb}, and\ u_{mc}$ are the phase modulation signals, u_{dc} is the DC bus voltage, $L_{s1}, R_{s1}, L_{s2}, R_{s2}, C_s\ and\ R_{s3}$ are the LCL filter parameters, and V_{abc} and $I_{abc}$are the AC voltages and currents.

As a result, the *in*verter VSG model can be written as:

$$\begin{cases} P^* + D_p(\omega^* - \omega_m) - P = J\omega^* \dfrac{d\omega_m}{dt} \\ Q^* + D_q(V^* - V) - Q = K \dfrac{dE_m}{dt} \end{cases} \quad (1)$$

P, Q are the *active and reactive power* at the AC bus with P^*, Q^* being the corresponding reference, V^* and V are the rated/ reference and real voltage amplitude of the AC voltage phasor, respectively, J, K are the inertia coefficients of the active and reactive power control loops, respectively, P, Q are the *active* and reactive power at the AC bus with P^*, Q^* being the corresponding reference, V^* and V are the rated/ reference and real V, ω^* and ωm are the VSG's rated/reference angular velocity and virtual rotor angular velocity, respectively; E_m and θ_m are the VSG's potential and phase.

The $P - f$ and $Q - V$ *d*roop characteristics, which are employed to simulate the *d*roop characteristics of the conventional SG, are used to derive E_m and θ_m in the VSG control in (1). After synthesizing the three-phase modulation signal u_m (containing the three independent modulation signals $u_{ma}, u_{mb}, and\ u_{mc}$), the grid-connected inverter is switched using Space Vector Pulse Width Modulation (SVPWM), as illustrated in Fig. 1. As a result, the predicted voltage and power may be managed, and *the* LCL filter can then provide it to the *AC bus*.

As you can see, the droop characteristic is as follows. The angular frequency ω_m drops as the load power P increases, ensuring steady-state operation of the angular frequency stability ($\frac{d\omega_m}{dt} = 0$). As a result, increasing P leads ω_m to drop. The relationship between reactive power Q and electric potential E_m is also similar.

III. DYNAMIC ANALYSIS OF VSG

The equivalent output impedance of the inverter, along with the line impedance, is indicated as $r + jX_s'$, where r and X_s' are the equivalent resistance and reactance, respectively. The output power is calculated as follows:

$$P\ +\ jQ = 3\mathrm{E}(\frac{E-V}{Z})^* = \frac{3}{2}\frac{E^2-EV(cos\delta + j\ sin\delta)}{r-jX_s'}$$

(2)

where E is the amplitude of the inverter output voltage phasor E and is the angle of *power* between $E\ and\ V$. The output power in (2) can be simplified Since $r \ll X's$.

$$P\ +\ jQ = \frac{3}{2}\frac{EV}{X_s'}sin\delta + j\frac{3}{2}\frac{E}{X_s'}(E-Vcos\delta)$$

$$\rightarrow \begin{cases} P = \frac{3}{2}\frac{E}{X_s'}sin\delta \\ Q = \frac{3}{2}\frac{E}{X_s'}(E-Vcos\delta) \end{cases}$$

(3)

This can be used in place of the VSG model of (1). It may be determined for the reactive power loop that

$$\begin{cases} Q^* + D_q(V^*-V) - \frac{3}{2}\frac{E}{X_s'}(E-Vcos\delta) = K\ \frac{dE_m}{dt} \\ E = K_{pwm}E_m, Q^* = 0 \end{cases}$$

(4)

$Kpwm$ denotes the PWM gain. When the system is functioning at steady-state, there is just a little disturbance around the rated, i.e., $\delta \approx 0$, which fits *the Taylor's theorem* requirements. As a result, putting $cos\delta \approx 1$ into (4) yields

$$D_q(V^*-V) - \frac{3}{2}\frac{E}{X_s'}(E-V) = \frac{K}{K_{pwm}}\frac{dE_m}{dt} \quad (5)$$

Similarly, for the active power, there are

$$\begin{cases} P^* + D_p(\omega^*-\omega_m) - \frac{3}{2}\frac{E}{X_s'}\ sin\delta = J_\omega^*\frac{d\omega_m}{dt} \\ \delta = \int(\omega_m - \omega^*)\ dt \end{cases}$$

(6)

which can be simplified considering $sin\delta \approx \delta$ as

$$J\omega^*\frac{d^2\delta}{dt^2} + D_p\frac{d\delta}{dt} + \frac{3}{2}\frac{EV}{X_s'}\ \delta = P^* \quad (7)$$

International Journal for Research in Applied Science & Engineering Technology (IJRASET)
ISSN: 2321-9653; IC Value: 45.98; SJ Impact Factor: 7.429
Volume 9 Issue XI Nov 2021- Available at www.ijraset.com

Then, the characteristic equation of (7) is given as

$$J\omega^* s^2 + D_p s + \frac{3}{2}\frac{EV}{X_s'} = 0 \qquad (8)$$

The *Laplace operator* is represented by the letter s. *The r*oot discriminant t Δ of (8) can be calculated as follows:

$$\Delta = (D_p)^2 - 4J\omega^* \cdot \frac{3}{2}\frac{EV}{X_s'} \qquad (9)$$

Because Dp is typically greater than 1000 W·s/rad and J is typically *less than* 0.058 kg•m², the first term of the right-hand side in (9), i.e., $(D_p)^2$,, is thousands of times greater than the other. Thus,

$$\Delta = (D_p)^2 - 6J\omega^* EI \approx (D_p)^2 \gg 0 \qquad (10)$$

I is the amplitude of the current injected into the PCC ($iabc$). As a result, the *roots* ρ of the characteristic equation in (8) can be calculated as follows:

$$\rho_{1,2} = \frac{-D_p \pm \sqrt{\Delta}}{2J\omega^*} < 0 \qquad (11)$$

This indicates that the system is always in grid-connected mode. The solution to (7) is then as follows:

$$\delta = C_1 e^{\frac{-D_p - \sqrt{\Delta}}{2J\omega^*}} + C_2 e^{\frac{-D_p + \sqrt{\Delta}}{2J\omega^*}} + \frac{2P^* X_s'}{3EV} \qquad (12)$$

with C_1 and C_2 being *constants* related to the primary states. *A*ccording to Eq. (3) and $sin\delta \approx \delta$, the output active power at the AC bus can be calculated with the primary conditions as

$$\begin{cases} P = \cdot\frac{3}{2}\frac{EV}{X_s'}(C_1 e^{\frac{-D_p - \sqrt{\Delta}}{2J\omega^*}} + C_2 e^{\frac{-D_p + \sqrt{\Delta}}{2J\omega^*}} + \frac{2P^* X_s'}{3EV}) \\ C_1 = -\frac{P^* X_s'}{3EV}\left(1 - \frac{D_p}{\sqrt{\Delta}}\right), C_2 = -\frac{P^* X_s'}{3EV}\left(1 + \frac{D_p}{\sqrt{\Delta}}\right) \end{cases} (13)$$

which can be simplified as

$$P = f_1(V,t) \qquad (14)$$

The preceding analysis implies that when the amplitude of the AC voltage changes by ΔV, the output potential changes by ΔE. As a result, ΔP will change the output active power. After the sample of the voltage V, the active power P, as a major yield parameter of the matrix connected activity, changes because of the control loop postponement and PWM switching delay. Subsequently, when the voltage magnitude is changed to distinguish islanding, the speed will be close to the switching frequency.

In any event, when the grid voltage changes significantly from the start, the above variety arrangement is as yet substantial, yet the particular measures might require further examination. In any case, the variety range of the voltage amplitude has no impact on the change arrangement among ΔV and ΔP, which clarifies why transformation successions instead of explicit limits are utilized in islanding recognition. The framework is changed to the islanding activity once islanding is affirmed. In the present circumstance, the response characteristic is momentarily inspected. In off-grid mode (i.e., islanding activity), the VSG reactive power loop can be depicted as

$$\begin{cases} Q^* + D_q(V^* - V) - Q = K\frac{dE_m}{dt} \\ V \approx E = K_{pwm}E_m , \frac{Q}{P} = tan\theta \end{cases} (15)$$

where θ is the power factor angle of the AC bus. Eq. (15) can be reduced to

$$Q^* + D_q(V^* - V) - P\,tan\theta = \frac{K}{K_{pwm}}\frac{dE}{dt}$$

$$(16)$$

The characteristic root of (16) is obtained as

$$\rho_3 = \frac{-D_q K_{pwm}}{K} < 0 \qquad (17)$$

which demonstrates that the framework will likewise work steadily and consistently in the off-lattice mode. The arrangement of (16) is then given as

$$\begin{cases} E = C_3 e^{-\frac{D_q K_{pwm}}{K}t} + \dfrac{Q^* + D_q V^* - Ptan\theta}{D_q} \\ C_3 = V^* - + \dfrac{Q^* + D_q V^* - Ptan\theta}{D_q} \end{cases} \qquad (18)$$

withC_3 being a constant as the initial condition. Considering $V \approx E,$ (18) can be $simplified$ as

$$V \approx E = f_2(P, t) \qquad (19)$$

It very well may be closed from the above investigation that the difference in the active power$r\Delta P$ prompts a variety of ΔE in the inverter yield voltage, and further actuates ΔV at the AC transport. Like the active power loop examination, consolidating with the control loop delay and PWM exchanging delay, the difference in the voltage magnitude$V$, as the controlled boundary in the off-framework activity mode, can be recognized after the testing of the active power$P$, even at the underlying stage with the extensive changes in power.

One more significant thing is that V is clasped by power grid when grid associated activity, and constrained by VSG in off-network mode. In other words, V will vibrate marginally at the time of detachment, and the subsidiary of(19) can likewise be utilized to recognize disconnected island.

As per (14) and (19), it is realized that the transformation succession of the voltage sufficiency changesΔV and the dynamic force varieties ΔP at the AC transport are diverse between the framework associated mode and the off-network mode (i.e., islanding). This is additionally summed up in Table 1.

A. *Proposed Islanding Detection Method*
As displayed in Fig. 2, a branch (signified as Branch 1) is planned in the proposed IDMto recognize the transformation grouping of the voltage changesΔV and the active power varieties ΔP to distinguish the off-network activity mode dependent on Table 1. Also, Branch 2 recognizes reactive power loop wavering by contrasting the pulses gathered in counter2, which is utilized to identify the transient cycle in Table 1. By and large, Branch 1 yields the islanding signal with extremely quick speed, and Branch 2 ensures the great repetition and unwavering quality. As shown in Fig. 2, the proposed technique utilizes equipment in DSP (i.e., counters and rising edge catch) to work on the islanding discovery. In the accompanying, the particular plan of the proposed IDM is detailed. 4.1. Plan of Branch 1 The transformation arrangement can be distinguished utilizing two switch-capacities. One identified with the outright difference in the AC transport voltage plentifulness, i.e., $|\Delta V| = |V^* - V|$, is planned as

$$f_v(|\Delta V|) = \begin{cases} 1, & |\Delta V| > |\Delta V|^* \\ 0, & |\Delta V| \le |\Delta V|^* \end{cases} \qquad (20)$$

where$|\Delta V|^*$ can be gotten by important force framework principles. Different relates to the dynamic outright change, i.e., $|\Delta P| = |P^* - P|$. It is additionally given as

$$f_p(|\Delta V|) = \begin{cases} 1, & |\Delta P| > |\Delta P|^* \\ 0, & |\Delta P| \le |\Delta P|^* \end{cases} \qquad (21)$$

in which $|\Delta P|^*$can be obtained as

$$|\Delta P|^* = 3 \frac{|\Delta P|^* I^*}{2} = P^* \frac{|\Delta V|^*}{V^*} \qquad (22)$$

when $f_p(|\Delta V|)$ = 1, the rising edge of $f_v(|\Delta V|)$ can be obtained by growing the edge get or counter1 in the DSP structure. Thusly, the structure works in the off-framework mode according to (19) and Table 1. If not, the system is in the network related movement mode according to (14).

Tolerating a power structure unsettling impact for example, when the power grid is disturbed(e.g., voltage drops),counter1 just yields the count beat right now of $|\Delta V| > |\Delta V|^*$. Nonetheless, $f_p(|\Delta P|)$= 0 as of now, and hence Branch 1 won't convey the islandingmessage. Just at the off-grid second when the transient required *power changes* to make $f_p(|\Delta P|)$= 1, Branch 1 yields the islanding signal as per Fig. 2. That is, Branch 1 can precisely recognize the off-framework second (i.e.,*the islanding second*) under various voltage unsettling influences.

B. Design of Branch 2

As displayed in the investigation of (19), V will vibrate marginally at the time of detachment, and the subsidiary of (19) can likewise be utilized to recognize separated island. In light of this trademark, a record ΔQ_q of the reactive power loop is characterized as

$$\Delta Q_q = Q^* + D_q(V^* - V) - Q \qquad (23)$$

That is, ΔQ_q is equivalent to 0, when the framework is working in steadystate. Likewise, a switch capacity can be plan as

$$f_Q(|\Delta Q_q|) = \begin{cases} 1, & |\Delta Q_q| > 0 \\ 0, & |\Delta Q_q| \le 0 \end{cases} \qquad (24)$$

The rising edge of $f_Q(|\Delta Q_q|)$is collected with over double the network central recurrence, and simultaneously, the pulse numberof the current yield ki is contrasted and the number $ki-1$ preceding a large portion of the crucial period. On the off chance that $K_i - K_{i-1} - KC_2 > 0$ the reactive power circle is wavering, and the framework is working in transient guideline measure as indicated by Table 1. Nonetheless, the reaction of Branch 2 is somewhat more slow than that of Branch 1 because of the constant counting.

Table 1
Mutation Sequence of ΔV and ΔP

Operation Mode	Mutation Sequence
Grid connected mode	$\Delta V \to \Delta E \to \Delta P$
At the off-grid moment	V oscillation
Off grid mode	$\Delta P \to \Delta E \to \Delta V$

To additionally exhibit the investigation, a basic case is exemplified in the accompanying. At the point when the neighborhood load equivalents to the evaluated power of the Inverter, $|\Delta P|$ and $|\Delta V|$ are too little to even consider setting off the discovery from Branch 1. That is, the standards of the change progression are invalid. Regardless, $Branch$ 2 really works reliably, and it can give the right $i$slanding signal by recognizing the analysis change of $the VSG$. In a word, Branch 2 can be used as the holdup of Branch 1to work on the dependability and excess of the proposed islanding identification approach for the VSG. The above judgment standards for the islanding discovery are additionally summed up in Table 2, which demonstrates when the comparing branch will work under the grid conditions.

Table 2
Judgment criteria of the proposed IDM.

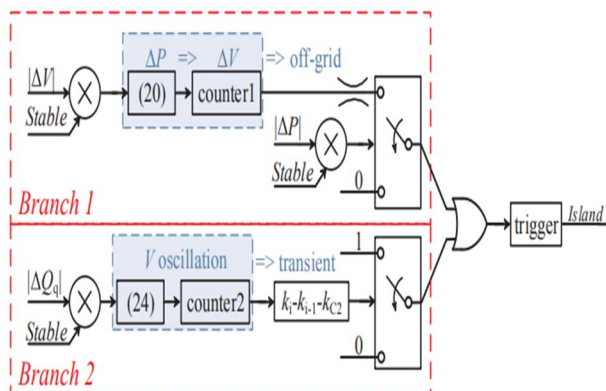| Branch	Condition	Operation mode
1	$f_p(|\Delta P|)$ rises and then $f_v(|\Delta V|)$	Off-grid
2	$K_i - K_{i-1} - K_{c2} > 0$	Off-grid
1 or 2	others	Grid connected

Fig. 2. Block diagram of the proposed islanding detection method, where "Stable" is the stable operation signal, "Island" is the islanding mode signal, K_i and K_{i-1} are the present and the last value of counter2, and KC_2 is the setting value difference.
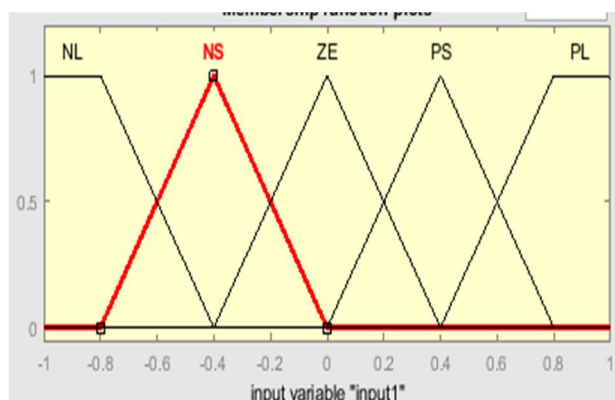
The legitimacy of the proposed plot comes from severe hypothetical deduction, and the identification precision doesn't rely upon boundary plan, which is likewise a significant benefit of the proposed conspire. $|\Delta V|^*$. in (20), recurrence in counters, and KC_2 are required in Fig. 2. $|\Delta V| *$. can be gotten by important power framework norms. Counter1 is utilized uniquely to recognize the rising edge of (20) and any recurrence can be utilized, in light of the fact that it just influence the identify point of the following shortcoming however not *the speed and precision* of this issue. The recurrence of Counter2 and KC_2 are utilized to identify V swaying. Since V is braced by power network when grid associated activity, any worth of recurrence and KC_2 can be utilized, and 100 Hz and 10 are embraced subsequent to thinking about the *reactive power* dynamic.

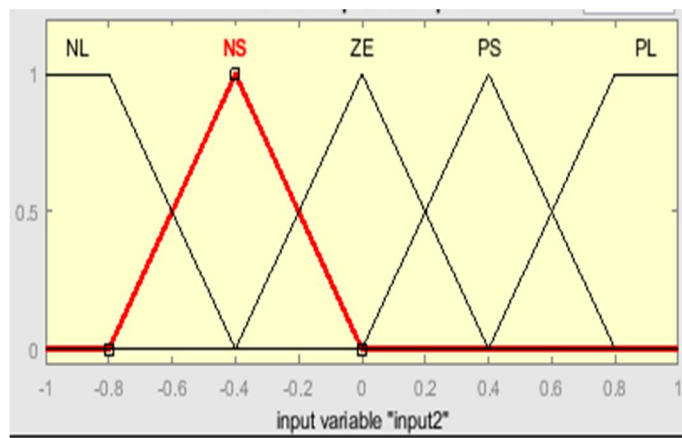*C. Controller Using Fuzzy Logic*

A fuzzy control system is a control structure subject to fuzzy $r$ationale—a logical system that examines straightforward data regards similarly as reasonable components that take on steady characteristics some place in the scope of 0 and 1, rather than old style or progressed rationale, which deals with discrete assessments of one or the other 1 or 0 (valid or bogus, independently). Fuzzy rationale is comprehensively used in machine control. The term $f$uzzyinsinuates the way that the rationale included can oversee thoughts that can't be imparted as the 'valid' or 'bogus' yet rather as somewhat evident'. But elective techniques, for instance, nonexclusive estimations and neural frameworks can perform correspondingly similarly as fuzzy rationale a large part of the time, fuzzy rationale has the favored position that the response for the issue can be tossed in phrasing that human executives can see, so their experience can be used in the construction of the regulator. This simplifies it to mechanize tasks that are at this point viably performed by individuals.

1) Fuzzy Sets: The enrollment elements of the Fuzzycontroller utilized in our reproduction model are given as pursues. The data factors in a *Fuzzy* control system are all things considered planned by sets of enlistment limits like this, known as Fuzzy sets. The way toward changing over a new data impetus to a *Fuzzy* worth is called $f$uzzification.
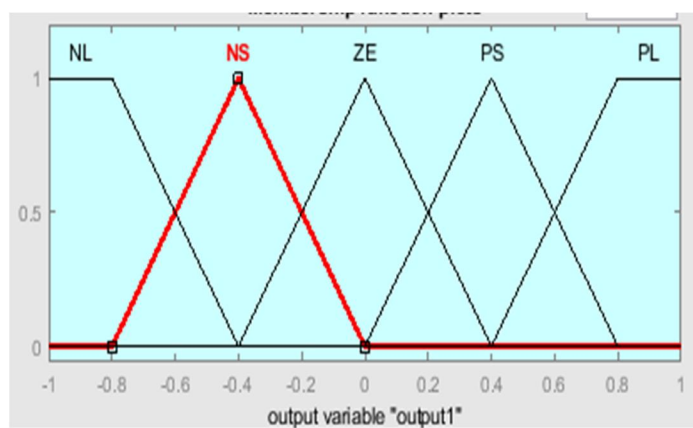
The enlistment components of the Fuzzy regulator used in our multiplication model are given as seeks after.

a) Input 1 Membership Function

International Journal for Research in Applied Science & Engineering Technology (IJRASET)
ISSN: 2321-9653; IC Value: 45.98; SJ Impact Factor: 7.429
Volume 9 Issue XI Nov 2021- Available at www.ijraset.com

b) Input 2 Membership Function

c) Output Membership Function

Fig 3 (a) Input 1 Membership Function, (b) Input 2 Membership Function, (c) Output Membership Function

D. Artificial Neural Network Artificial

$Neural\ Network\ (ANN)$ is a smart framework that adjusts effectively to non-direct and surprisingly conceptual frameworks by finding out with regards to them through a set of preparing information. The ANNis includes with enormous number of neurons which is called as parallel and circulated handling framework. It utilizes a solitary *or* multi-layer feed-forward network. The multi-layer feed forward engineering comprises of info and yield layer joined with at least one secret layer. Radial Basis Network calculation is the foundation of the *ANN* preparing measure. The inclination plummet method can be usedto limit the expense work is equivalent to $Mean\ Squared\ Error\ (MSE)$ which is characterized as the contrast between the ideal yields and the real organization yields. Multi-dimensional planning issues can likewise be handily dealt with utilizing a multi-layer feed forward network. A two-layer network is displayed as a specific model in Fig. 4. It comprises of information neutron and yield the one layer of sigmoid secret neurons is set in the middle of the info neurons and the other layer of direct yield neurons. The yield neuron is the capacity of the weighted amount of the sources of info neuron alongside the predisposition is follows:

$$y_j = f\left[\left(w_{ij}x_{ij}\right) + b_j\right] \qquad (25)$$

As referenced, the $layered\ feed-forward\ ANNs$ is prepared by the Radial Basis networkcalculation. The information neurons convey their messages forward, and afterward the mistakes are proliferated in reverse to change the loads. To initiate the network, directed learning procedure is utilized in the Radial Basis Network calculation, from which the mistake is determined. The mistake is the contrast among genuine and expected yields and it very well may be determined by calculation with set of information sources and yields. This mistake is diminished by utilizing Radial Basis Networkcalculation until the ANN learns the preparation information. The critical factor of ANN is to prepare information with irregular loads and change them to limit the blunder.
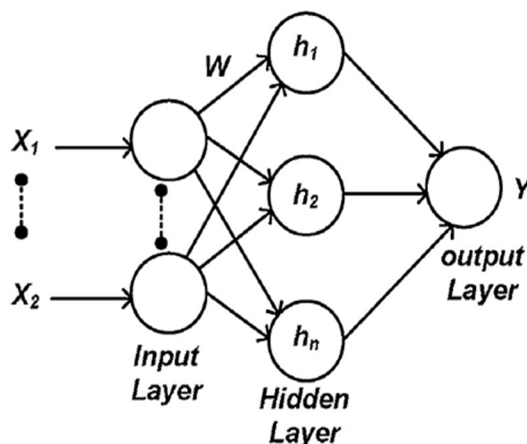
International Journal for Research in Applied Science & Engineering Technology (IJRASET)
ISSN: 2321-9653; IC Value: 45.98; SJ Impact Factor: 7.429
Volume 9 Issue XI Nov 2021- Available at www.ijraset.com

Fig. 4. Architecture of feed forward network.

IV. SIMULATION RESULTS

To check the adequacy of the proposed techniques, *simulations* have been completed in *MATLAB/ Simulink*.The total framework is displayed in Fig. 1. At the point when the distribution network falls flat, the microgrid framework is separated from the power grid and works in an arbitrary island with obscure required power

A. Simulation Results using PI controller

1) *Weak Coupling Of Power Loops:* Right off the bat, the frail coupling between the $P - f$ and $Q - V$ droop attributes is displayed underneath. For this situation, $P^* = 10$ kW, $Q^* = 0$ kVar, and the grid voltage drops to 0.9p.u. from $2.5\ s\ to\ 3.125\ s$. Fig. 5(b) and Fig. 5(c) shows that the active and reactive powersway with a similar example both at $t = 2.5\ s\ and\ t = 3.125\ s$, which is the power coupling wonder of the VSG. In Fig. 5(c), the reactive power incrementsto $320*155*1.414*0.1 = 7014.5$ Var (0.7p.u.), which is reliable with (1).
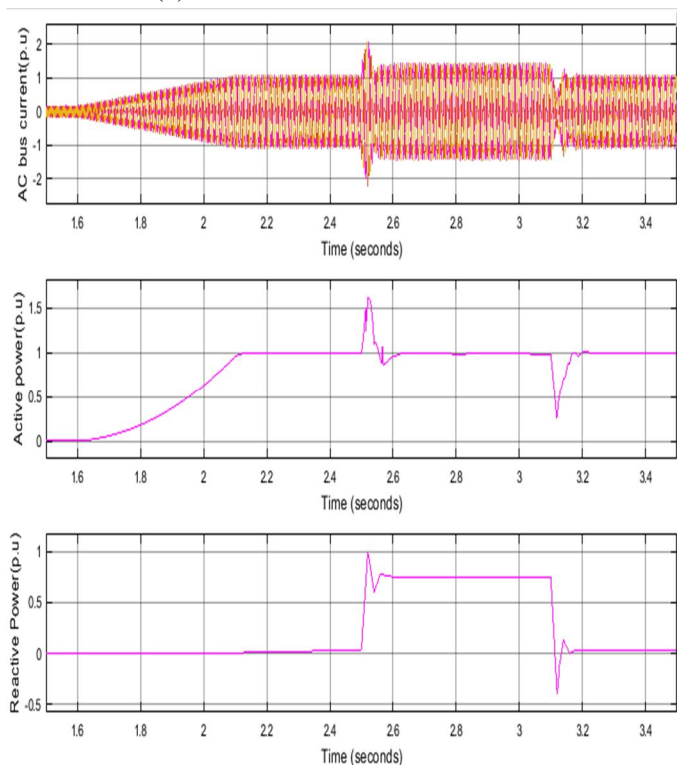

Fig. 5. Simulation results of weak coupling: (a) AC bus current, (b) output active power, and (c) output reactive power.

2) *Performance under Grid Disturbances:* For this situation, $P^* = 10\ kW$, and the local load power P_L = 5 kW. The reproduction results are displayed in Fig. 6. As seen in Fig. 6(a), the lattice voltage drops to 0.9p.u. from 2.5 s to 2.65 s and from 2.7 s to 2.95 s, and the framework is disconnected from the network at t = 3 s. The fluctuation of the AC bus voltage $vabc$ is little at t = 3 s in Fig. 6(a), and the *inverter does*n't cause any huge voltage sway on *t*he AC bus and local load when the new switching control calculation is embraced. Besides, *a*s displayed in Fig.6(b),the proposed IDM can in any case guarantee an appropriate activity on account of high frequency disturbances from from 2.5 s to 2.95 s. All the more explicitly, it can distinguish the off-lattice second precisely at t = 3 s, which affirms the conversations in Area 3.1. As As $|\Delta V|\ and\ |\Delta P|$ change right away, the discovery takes a couple of milliseconds, when *the proposed strategy* is taken on. The *two branches are* powerful, however the reaction of Branch 2 is somewhat more slow than Branch 1, as examined in Segment 3. Thusly, the reenactment confirms that the proposed IDM has great repetition and unwavering quality. Moreover, the $Q - V positive\ feedback\ method$. For the benchmarked dynamic IDM, the thought is to have the recurrence effect at $AC\ bus$ continuously way to deal with a pre-set worth, and afterward the islanding signal is created. As seen in Fig. 4(c), the course of this *d*ynamic IDM is additional tedious contrasted with the proposed method,while the proposed IDM dependent on VSG activity attributes shows better execution.
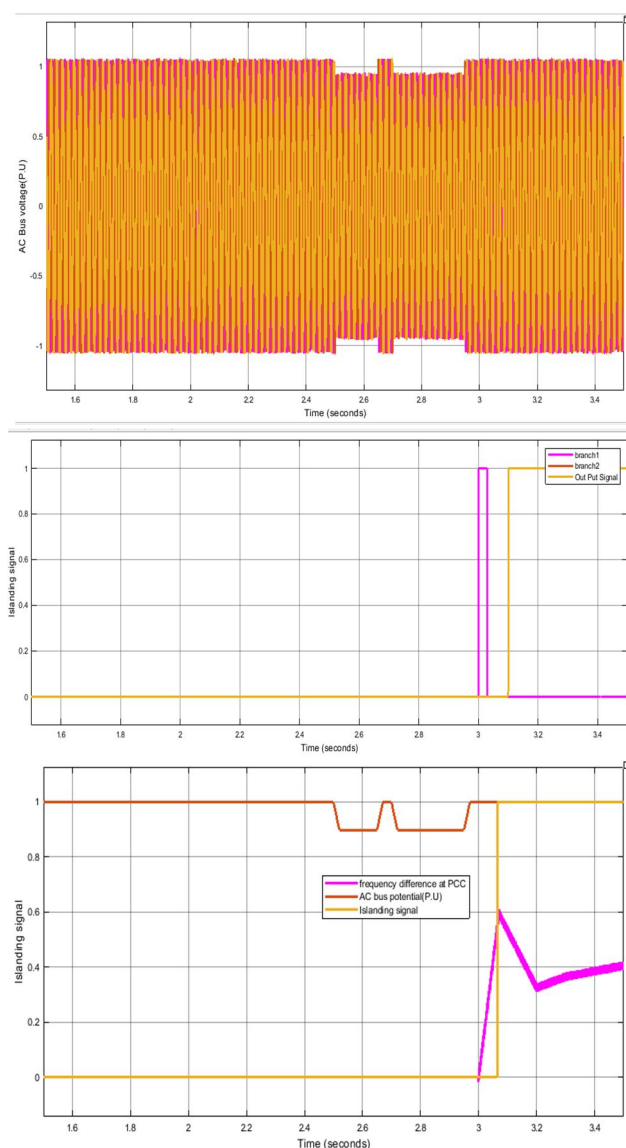

Fig. 6. Simulation results under grid disturbances: (a) AC bus voltage, (b) output signal of the proposed IDM, and (c) results of a prior-art active IDM using the Q-V positive feedback.

3) *Performance under LVRT:* The islanding issue might happen arbitrarily whenever, additionally during the time spent LVRT, however the IDM and LVRT calculation for the most part run thus in turn framework. For instance, Fig. 7 is decided to be LVRT from 2.5 s to 3.125 s, yet the disconnected island occurs at 3 s, so the framework needs to recognize the off-grid second under LVRT mode. For this situation, $P^* = 10$ kW, and $P_L = 5$ kW. The low voltage ride-through (LVRT) calculation introduced is taken on to check the adequacy of the *proposed IDM*. As confirmed in Fig. 7(a), the framework voltage drops to $0.2 p.u. during$ $2.5 - 3.125$ s, however the framework *is* disengaged from the grid at $t = 3$ s. Furthermore, the difference in the yield *power ΔP causes the voltage variety ΔV at t = 3 s*, which concurs with the investigation in (19). As it very well may be seen in Fig. 7(b), the yield current of the *g*rid associated inverter is steady under the LVRT activity, and the effect isn't created at the time moments of 2.5 s and 3 s. At the point when the framework is disengaged from the power grid at $t = 3$ s, the transient timeframe doesn't create critical current tops because of the immediate power varieties. In this manner, there is no danger to trigger the overcurrent assurance to close down the whole framework, and the consistent state yield current is steady in the islanding activity mode. Additionally, as it is displayed in Fig. 7(c), the proposed calculation doesn't misjudge the islanding condition at t = 2.5 s, as the framework is working under the LVRT condition. At the end of the day, the proposed IDM can work with the LVRT calculation at the same time and distinguish the offgrid condition precisely and dependably. Contrasting and existing technique, Fig. 7(d) shows Q-V positive criticism can recognize the island with more slow speed due to the progression change of recurrence contrast.
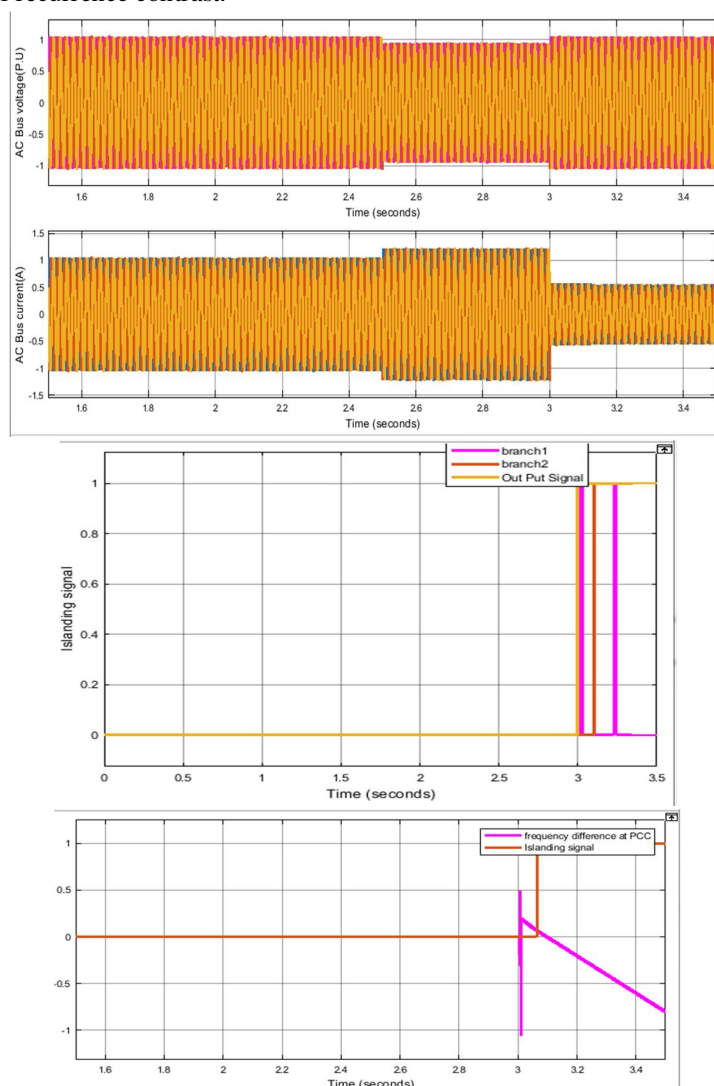

Fig. 7. Simulation results of the system operating under the low-voltage ridethroughoperation: (a) AC bus voltage, (b) AC bus current, (c) output signal of the proposed IDM, and (d) results of Q-V positive feedback.

4) *Performance under a Quality Factor of 2.5:* For this situation, $P^* = 5\ kW$, the nearby burden $P_L = 5$ kW, $QL_c = 12.5$ kVar, and $QL_L = 12.5\ kVar$, and the power framework is disconnected at t= $3\ s$. The quality factor *is* 2.5 under the present situation, which is one of the common instances of *i*slanding. The simulation results are displayedin Fig. 8. As seen in Fig. 8(a), the AC transport voltage vabc has irrelevant varieties, and ΔV can scarcely be identified to trigger Branch 1 at t = 3 s. Moreover, Fig. 8(b) exhibits that the power contrast ΔQ_q has high-recurrence motions and deviates a long way from its base worth at the time moment of the off-framework, which is reliable with the examination of (23) and (24). As displayed in Fig. 8(c), Branch 1 neglects to identify the off-grid situation when the necessary burden is equivalent to the *a*ppraised yield power (i.e., the quality factor being 2.5), however the islanding sign of Branch 2 guarantees the location due to the high recurrence transient motions of ΔQ_q. Subsequently, the reactive power wavering can be chosen as an identification file with high dependability through Branch 2. Taking all things together, the recreations further affirm that the proposed calculation is viable.
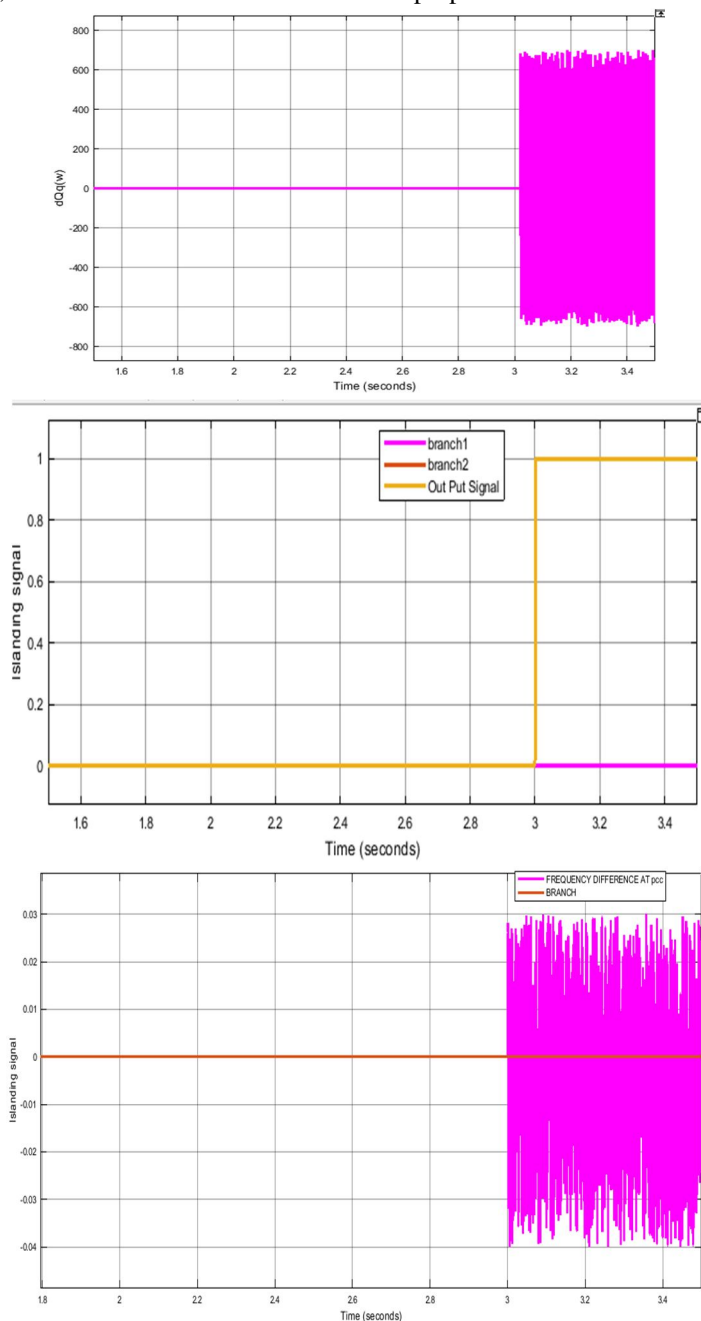

Fig. 8. Simulation results under a quality factor of 2.5: (a) AC bus voltage, (b) ΔQq waveform, and (c) output signal of the proposed IDM, and (d) results of Q-V positive feedback.

International Journal for Research in Applied Science & Engineering Technology (IJRASET)
ISSN: 2321-9653; IC Value: 45.98; SJ Impact Factor: 7.429
Volume 9 Issue XI Nov 2021- Available at www.ijraset.com

B. *Simulation Results using Fuzzy Controller*

1) *Weak Coupling of Power Loops:* Right off the bat, the frail coupling between the $P - f$ and $Q - V$ droopattributes is displayed underneath. For this situation, P^*= 10 kW, $Q^* = 0$ kVar, and the grid voltage drops to $0.9 p.u.$ from $2.5\ s$ to $3.125\ s$. Fig. 9(b) and Fig. 9(c) shows that the active and reactive power sway with a similar example both at t = 2.5 s and t = 3.125 s, which is the power coupling wonder of the VSG. In Fig. 9(c), the reactive power increments to 320*155*1.414*0.1 = 7014.5 Var (0.7p.u.), which is reliable with (1).
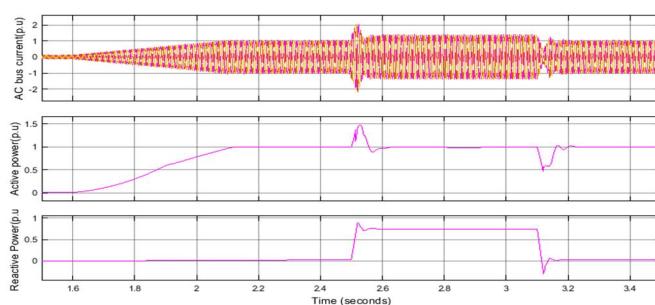
Fig. 9. Simulation results of weak coupling: (a) AC bus current, (b) output active power, and (c) output reactive power.

2) *Performance Under Grid Disturbances:* For this situation, P^*= 10 kW, and the local load powerP_L= 5 kW. The reproduction results are displayed in Fig. 10. As seen in Fig. 6(a), the lattice voltage drops to 0.9p.u. from 2.5 s to 2.65 s and from 2.7 s to 2.95 s, and the framework is disconnected from the network at t = 3 s. The fluctuation of the AC bus voltage$vabc$ is little at t = 3 s in Fig. 10(a), and the *inverter does*n't cause any huge voltage sway on the AC bus and local load when the new switching control calculation is embraced. Besides, *a*s displayed in Fig.10(b),the proposed IDM can in any case guarantee an appropriate activity on account of high frequency disturbances from from $2.5\ s$ to $2.95\ s. A$ll *t*he more explicitly, it can distinguish the off-lattice second precisely at t = 3 s, which affirms the conversations in Area 3.1. As As$|ΔV|$ *and* $|ΔP|$ change right away, the discovery takes a couple of milliseconds, when *the proposed strategy* is taken on. The *two branches are* powerful, however the reaction of Branch 2 is somewhat more slow than Branch 1, as examined in Segment 3. Thusly, the reenactment confirms that the *proposed IDM* has great repetition and unwavering quality. Moreover, the $Q - V$ positive feedback method .
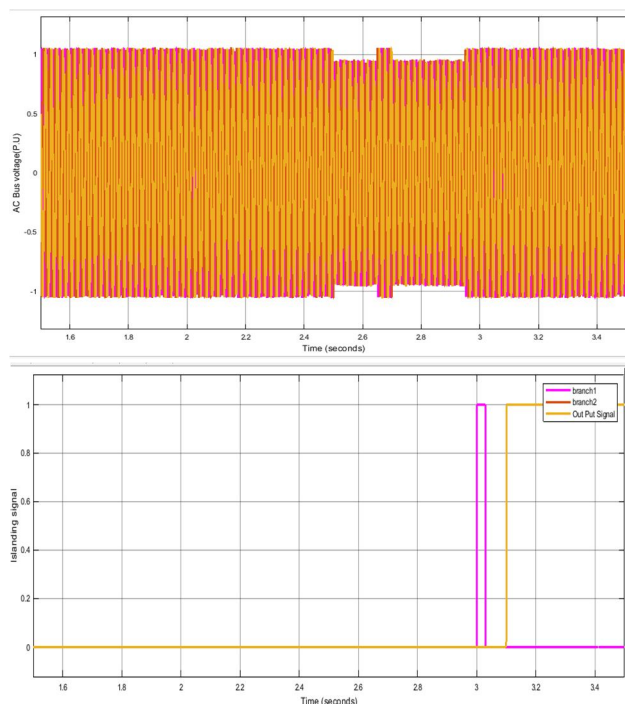

Fig. 10. Simulation results junder grid disturbances: (a) AC bus voltage, (b) output signal of the proposed IDM

3) *Performance under LVRT:* Theislanding issue might happen arbitrarily whenever, additionally during the time spent $LVRT$, however the IDM and LVRT calculation for themost part run thus in turn framework. For instance, Fig.11 is decided to be LVRT from $2.5\ s\ to\ 3.125\ s$, yet the $d$isconnected island occurs at $3\ s$, so the framework needs to recognize the off-grid second under LVRT mode. For this situation, $P* = 10\ kW$, and $PL = 5\ kW$.The low voltage ride-through (LVRT) calculation introduced is taken on to check the adequacy of the proposed IDM. As confirmed in Fig. 11(a), the framework voltage drops to 0.2p.u. during 2.5–3.125 s, however the framework is disengaged from the grid at t = 3 s. Furthermore, the difference in the yield power ΔP causes the voltage variety $\Delta V\ at\ t = 3\ s$, which concurs with the investigation in (19). As it very well may be seen in Fig. 11(b), the yield currentof the grid associated inverter is steady under the LVRT activity, and the effect isn't created at the timemoments of 2.5 s and 3 s. At the point when the framework is disengaged from the force grid at t = 3 s, the transient time frame doesn't create critical current tops because of the immediate power varieties. In this manner, there is no danger to trigger the overcurrent assurance to close down the whole framework, and the consistent state yield current is steady inthe islanding activity mode.
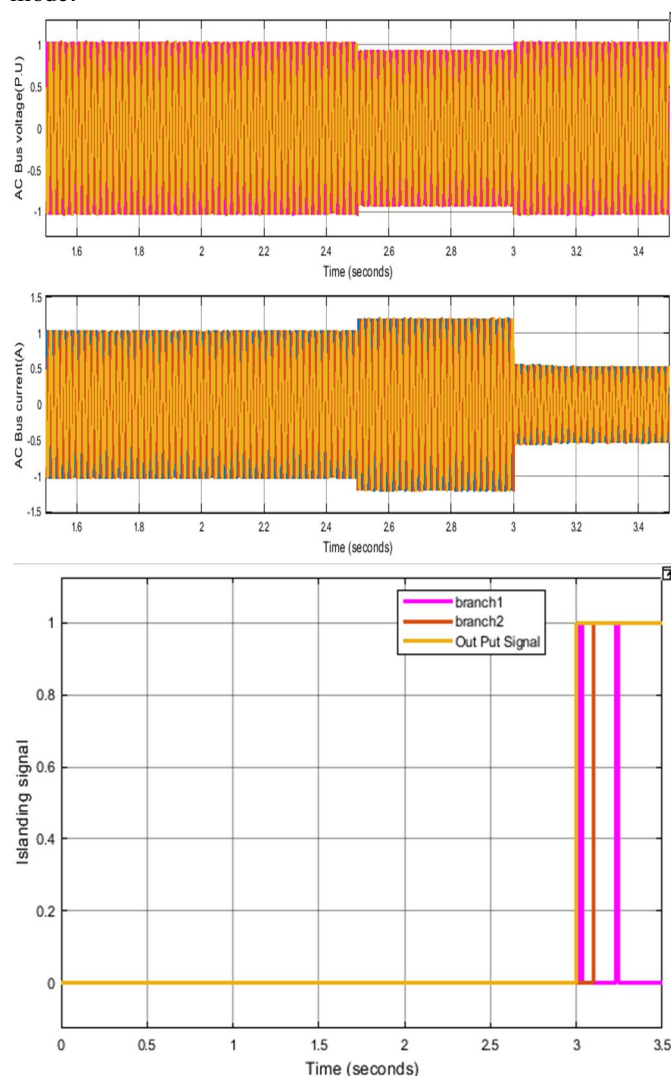

Fig. 11. Simulation results of the system operating under the low-voltage ridethrough operation: (a) AC bus voltage, (b) AC bus current, (c) output signal of the proposed IDM,

Additionally, as it is displayed in Fig. 11(c), the proposed calculation doesn't misjudge the islanding condition at t = 2.5 s, as the framework is working under the LVRT condition. At the end of the day, the proposed IDM *can work with the*LVRT calculation at the same time and distinguish the offgrid condition precisely and dependably.

4) *Performance Under a Quality Factor of 2.5:* For this situation, $P^* = 5$ kW, the nearby burden $P_L = 5$ kW, $QL_c = 12.5$ kVar, and $QL_L = 12.5$ kVar, and the power framework is disconnected at t=3 s. The quality factor is 2.5 under the present situation, which is one of the common instances of islanding. The simulation results are displayed in Fig. 12. As seen in Fig. 12(a), the AC transportvoltage vabc has irrelevant varieties, and ΔV can scarcely be identified to trigger Branch 1 at t = 3 s. Moreover, Fig. 12(b) exhibits that the power contrastΔQ_qhas high-recurrence motions and deviates a long way from its base worth at the time moment of the off-framework, which is reliable with the examination of (23) and (24).
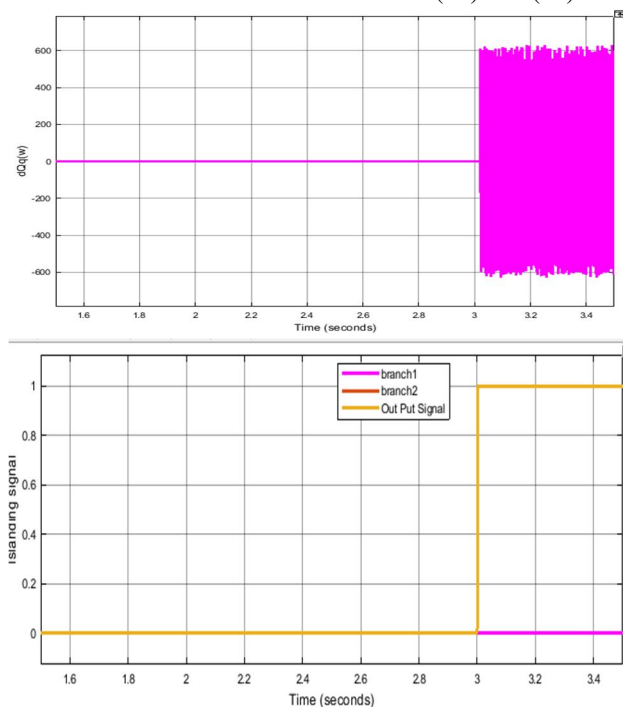

Fig. 12. Simulation results under a quality factor of 2.5: (a) AC bus voltage, (b) ΔQq waveform

C. *Simulation Results using Neural Networks*

1) *Weak Coupling of Power Loops:* Right off the bat, the frail coupling between the $P - f$ and $Q - V$ droop attributes is displayed underneath. For this situation, $P^* = 10$ $kW, Q^* = 0$ kVar, and the grid voltage drops to $0.9 p.u.$ from 2.5 s to 3.125 $s. Fig. 13(b)$ and $Fig. 13(c)$ shows that the active and reactive power sway with a similar example both at t = 2.5 s and t = 3.125 s, which is the power coupling wonder of the VSG. In Fig. 13(c), the reactive power increments to $320 * 155 * 1.414 * 0.1 = 7014.5$ Var $(0.7 p.u.), w$hich is reliable with (1).
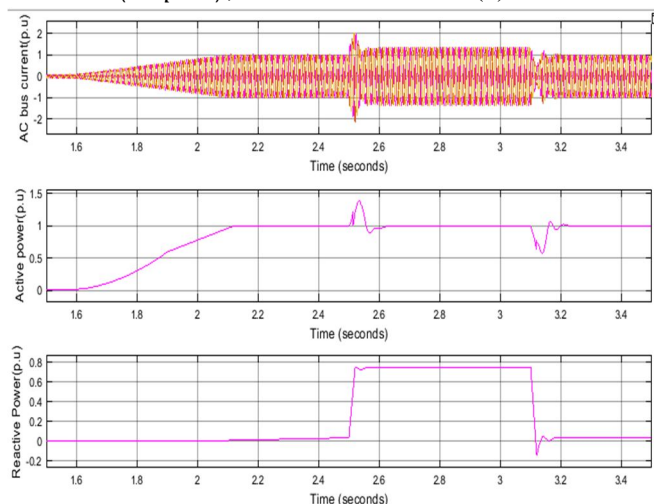

Fig13. Simulation results of weak coupling: (a) AC bus current, (b) output active power, and (c) output reactive power.

2) *Performance under grid Disturbances:* For this situation, P^*= 10 kW, and the local load powerP_L= 5 kW. The reproduction results are displayed in Fig. 14. As seen in Fig. 14(a), the lattice voltage drops to 0.9p.u. from 2.5 s to 2.65 s and from 2.7 s to 2.95 s, and the framework is disconnected from the network at t = 3 s. The fluctuation of the AC bus voltage$vabc$ is little at t = 3 s in Fig. 14(a), and the inverter doesn't cause any huge voltage sway on the AC bus and local load when the new switching control calculation is embraced. Besides, as displayed in Fig.14(b),the proposed IDM can in any case guarantee an appropriate activity on account of high frequency disturbances from from $2.5\ s\ to\ 2.95\ s$. All *t*he more explicitly, it can distinguish the off-lattice second precisely at t = 3 s, which affirms the conversations in Area 3.1. As As $|\Delta V|\ and\ |\Delta P|$ change right away, the discovery takes a couple of milliseconds, when the proposed strategy is taken on. The two branches are powerful, however the reaction of Branch 2 is somewhat more slow than Branch 1, as examined in Segment 3. Thusly, the reenactment confirms that the proposed IDM has great repetition and unwavering quality. Moreover, the $Q-V$positive feedback method .
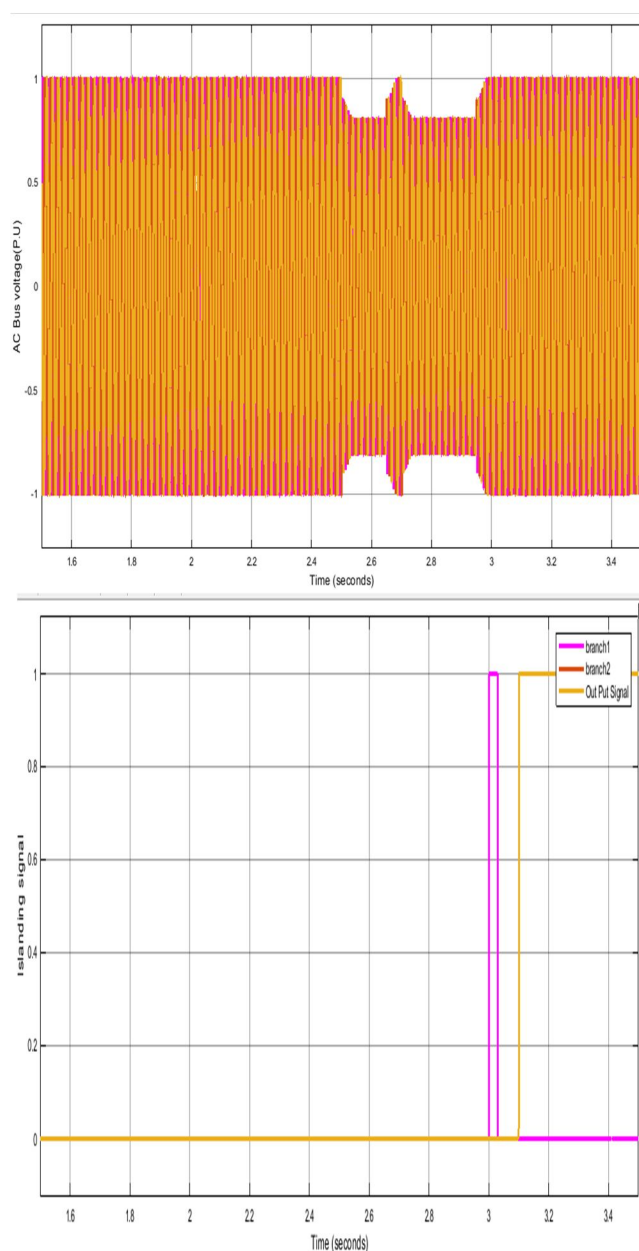

Fig. 14. Simulation results under grid disturbances: (a) AC bus voltage, (b) output signal of the proposed IDM

3) *Performance under LVRT:* The islanding issue might happen arbitrarily whenever, additionally during the time spent *LVRT*, however *t*he IDM and LVRT calculation for the most part run thus in turn framework. For instance, $Fig.$15 is decided to *be* LVRT from $2.5\ s\ to\ 3.125\ s$, yet the disconnected island occurs at 3 s, so the framework needs to recognize the off-grid second under LVRT mode. For this situation, P^*= 10 kW, and P_L = 5 kW. The low voltage ride-through (LVRT) calculation introduced is taken on to check the adequacy of the proposed IDM. As confirmed in Fig. 15(a), the frameworkvoltage drops to $0.2p.u.$ during $2.5-3.125\ s$, however the framework is disengaged from the grid at t = 3 s. Furthermore, the difference in the yield power ΔP causes the voltage variety $\Delta V\ at\ t\ =\ 3\ s$, which concurs with the investigation in (19). As it very well may be seen in Fig. 15(b), the yield current of the grid associated inverter is steady under the LVRT activity, and the effect isn't created at the time moments of 2.5 s and 3 s. At the point when the framework is disengaged from the force grid at t = 3 s, the transient time frame doesn't create critical current tops because of the immediate power varieties. In this manner, there is no danger to trigger the overcurrent assurance to close down the whole framework, and the consistent state yield current is steady inthe islanding activity mode. Additionally, as it is displayed in Fig. 15(c), the proposed calculation doesn't misjudge the islanding condition at t = 2.5 s, as the framework is working under the LVRT condition. At the end of the day, the proposed IDMcan work with the LVRT calculation at the same time and distinguish the offgrid condition precisely and dependably.
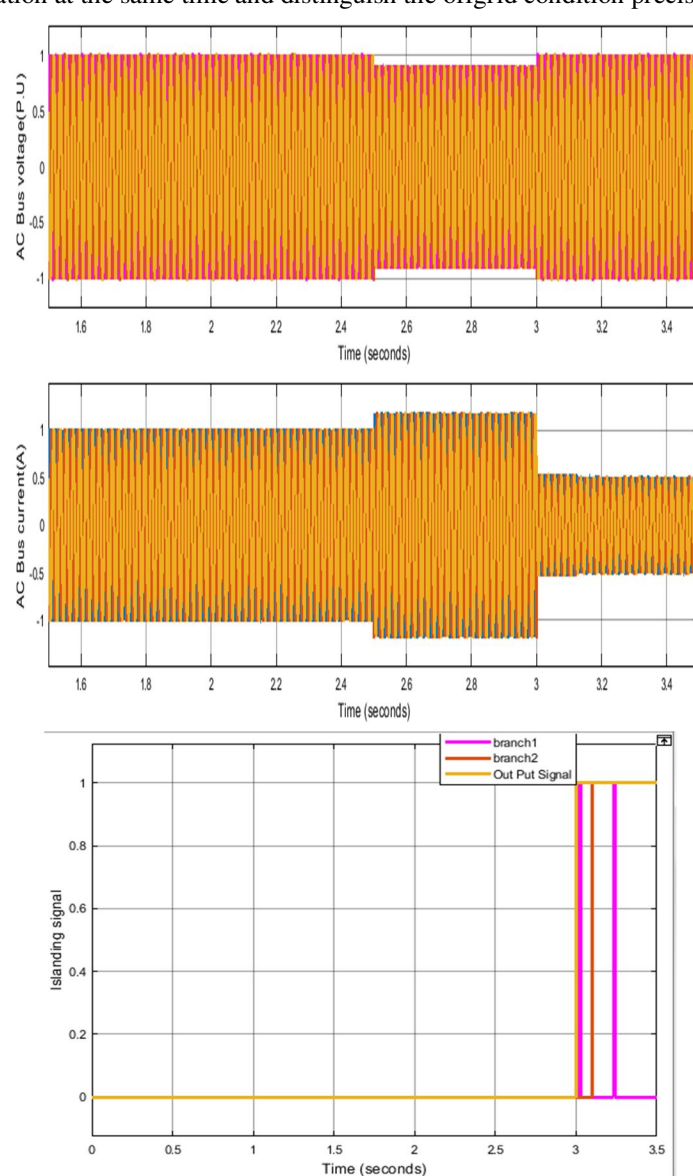

Fig. 15. Simulation results of the system operating under the low-voltage ridethrough operation: (a) AC bus voltage, (b) AC bus current, (c) output signal of the proposed IDM,

4) *Performance under a quality factor of 2.5:* For this situation, P∗ = 5 kW, the nearby load $PL = 5\,kW, QLc = 12.5\,kVar, and\,QLL = 12.5$ kVar, and the power framework is disconnected at $t = 3\,s$. The quality factor is 2.5 under the present situation, which is one of the common instances of islanding. The simulation results are displayed in Fig. 16. As seen in Fig. 16(a), the AC transport voltage $vabc$ has irrelevant varieties, and ΔV can scarcely be identified to trigger Branch 1 at t = 3 s. Moreover, Fig. 16 b) exhibits that the power contrast ΔQ_q has high-recurrence motions and deviates a long way from its base worth at the time moment of the off-framework, which is reliable with the examination of (23) and (24).
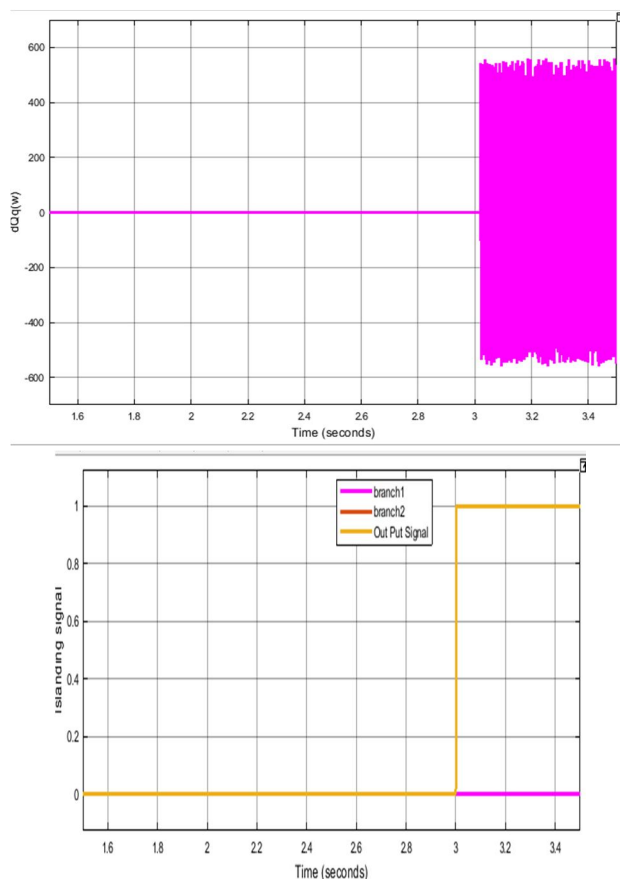

Fig. 16. Simulation results under a quality factor of 2.5: (a) AC bus voltage, (b) ΔQq waveform

THD comparison table: 3

parameter	PI	fuzzy	NN
Current(case1)	6.15%	3.4%	1.23 %
Voltage(case2)	5.5%	3.50%	1.24%
Voltage and current(case3)	5.51 % and 4.24%	3.68 % and 2.90%	1.11 % and 1.06%

V. CONCLUSION

This research suggested a new passive IDM that can accurately and quickly detect islanding in a variety of complex situations. The relationship between the P-f and Q-V droop characteristics was investigated to show that the off-grid change sequence of the AC bus voltage amplitude and the output active power varies. According to simulation data, the proposed NN-based IDM can efficiently identify islanding under multiple grid disturbances, LVRT, and a quality factor of 2.5 in a matter of milliseconds, which is substantially faster than the IEEE Std. 1547's 2 s. And also proposed NN based IDM controllers provide better performance as compared with the PI and Fuzzy controllers

REFERENCES

[1] Teodorescu R, Liserre M. 'Grid converters for photovoltaic and wind power systems'. 1st ed. Beijing, China: China Machine Press; 2015. p. 84–110.

[2] Dhar S, Dash P. Harmonic profile injection-based hybrid active islanding detection technique for PV-VSC -based microgrid system. IEEE T. Sustain. Energ. 2016;7(4):1473–81.

[3] Gupta P, Bhatia R, Jain D. Average absolute frequency deviation value based active islanding detection technique. IEEE T. Smart Grid 2014;6(1):26–35.

[4] Jia K, Wei H, Bi T, Thomas D. An islanding detection method for multi-DG systems based on high-frequency impedance estimation. IEEE T. Sustain. Energ. 2017;8(1):74–83.

[5] Hamzeh M, Rashidirad N, Sheshyekani K, Afjei E. A new islanding detection scheme for multiple inverter-based DG systems. IEEE T. Energy Conver. 2016;31(3):1002–11.

[6] Samui A, Samantaray S. Assessment of ROCPAD relay for islanding detection in distributed generation. IEEE T. Smart Grid 2011;2(2):391–8.

[7] Geng H, Xu D, Wu B, Yang G. Active islanding detection for inverter-based distributed generation systems with power control interface. IEEE T. Energy Conver. 2011;26(4):1063–72.

[8] Ray P, Kishor N, Mohanty S. Islanding and power quality disturbance detection in grid-connected hybrid power system using wavelet and s-transform. IEEE T. Smart Grid 2012;3(3):1082–94.

[9] Mohanty S, Kishor N, Ray P, Catalo J. Comparative study of advanced signal processing techniques for islanding detection in a hybrid distributed generation system. K. Shi, et al. Electrical Power and Energy Systems 123 (2020) 106277 8IEEE T. Sustain. Energ. 2014;6(1):122–31.

[10] Narayanan K, Siddiqui S, Fozdar M. Hybrid islanding detection method and priority-based load shedding for distribution networks in the presence of DG units. IET Gener. Transm. Dis. 2017;11(3):586–95.

INTERNATIONAL JOURNAL
FOR RESEARCH

IN APPLIED SCIENCE & ENGINEERING TECHNOLOGY

Call : 08813907089   (24*7 Support on Whatsapp)